OVERVIEW OF THE PINHOLE CAMERA DESIGN
FOR THE DIAMOND-II UPGRADE

N. Vitoratou*, L. Bobb, Diamond Light Source, Didcot, UK

Abstract

Pinhole cameras serve as the primary diagnostic for emittance and energy spread measurements in the storage ring of Diamond Light Source. Similar pinhole cameras will be employed for the Diamond-II upgrade, to enable direct imaging of the stored beam while also allowing for the monitoring of skew, profile, position, and instabilities. The emittance and energy spread are calculated from the acquired beam size measurement, combined with the lattice parameters. In this paper, an overview of the new system for Diamond-II is presented. The changes and upgrades made to the existing setup, the challenges and the choice of the different components are described. Additionally, future work that could improve the performance of the system is explored.

INTRODUCTION

The Diamond-II upgrade aims to transform the existing Double Bend Achromat lattice into a Multi Bend Achromat, reducing the natural horizontal emittance of the electron beam from 2700 pm.rad to 163 pm.rad, thus enhancing the brightness and the coherence of the synchrotron radiation [1].

X-ray pinhole cameras (XPCs) are deployed for transverse profiling of the electron beam in the storage ring as they offer direct 2D imaging of the stored beam, reliability and sufficient spatial resolution to measure the expected nominal beam sizes in Diamond-II [2, 3]. For a squeezed beam following optics correction, the estimated vertical emittance is 1 pm.rad, resulting in a beam size of 4 µm at the source points [1]. For this range of beam size that are below the pinhole cameras resolution, X-ray diffractometry has been tested in Diamond and can be used as a complementary technique [4]. Although, the design of the XPC system for Diamond-II will be based on the existing design, new challenges have arisen and need to be addressed. In parallel, improvements of the system will be accounted in the design.

SOURCE POINT SELECTION

Using two transverse beam size monitors located at different positions in the storage ring with different lattice parameters, the emittance and the energy spread in the ring can be calculated in the horizontal and the vertical plane. Two source points have been selected: dipole D1, a longitudinal-gradient bend supplying the X-ray beam to Pinhole Camera 1, and dipole D4, a constant-gradient bend supplying the X-ray beam to Pinhole Camera 2 [1]. The X-ray beam is extracted at 4 mrad and 7.2 mrad into the magnet bend respectively, ensuring clearance from the fringe-field region.

---

* niki.vitoratou@diamond.ac.uk

The beamline configuration has been verified to prevent any background radiation from upstream components. The corresponding source and lattice parameters for these bending magnets are summarised in Table 1.

Table 1: Parameters of D1 and D4 Bending Magnets and Nominal Beam Conditions

Parameter	D1	D4
Magnetic field	0.83 T	0.7 T
Critical energy	6818 eV	6103 eV
Total power per mrad	44.9 Watts	40.6 Watt
Horiz beta function	1.613 m	0.708 m
Vert beta function	19.858 m	10.306 m
Horiz dispersion	2.21 mm	10.04 mm
Horiz emittance	160 pm rad	
Vert emittance	8 pm rad	
Energy spread	0.00094	
Horiz beam size	16.3 µm	14.2 µm
Vert beam size	12.6 µm	9.1 µm

PINHOLE CAMERA SETUP

The X-ray pinhole camera setup consists of a bending magnet source, the pinhole aperture at distance d_0 from the source and a scintillating screen at distance d_i downstream of the pinhole, which forms the image of the source. The visible light image from the scintillator screen is then relayed through an optical lens onto the camera sensor (see Fig. 1).
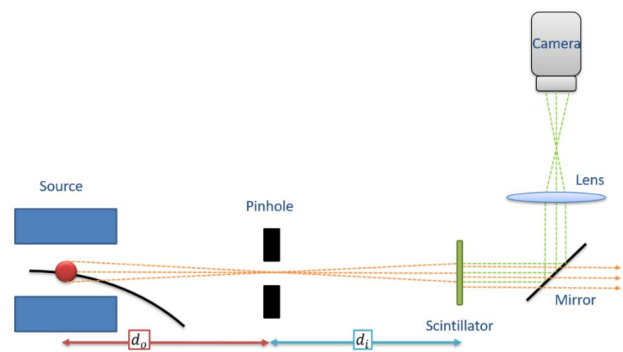

Figure 1: X-ray pinhole camera layout, including source, pinhole aperture, scintillator, mirror, lens, and camera.

The distances for the two pinhole cameras systems and the corresponding magnification $M = d_i/d_0$ are given in the Table 2. To achieve the highest possible magnification, pinhole apertures will be placed as close as possible to the

source point and the imaging system as far downstream along the beamline as possible. For Diamond-II the pinhole apertures will be placed about 1 m closer to the source point in comparison to the design of Diamond, while the imaging system will remain at the end of the beamline, resulting in higher magnification of the pinhole cameras.

Table 2: Magnfication for Pinhole Cameras

Source Point	Distance d_0	Distance d_i	Mag
D1	2.7 m	13.3 m	4.9
D4	3.0 m	12.5 m	4.2
Diamond	4 m	10 m	2.5

The minimum resolvable beam size σ_{min} at the source is estimated analytically as [5]:

$$\sigma_{min} = \sqrt{\frac{\lambda d_0}{2\sqrt{(3)}}\frac{d_0 + d_i}{d_i}}, \tag{1}$$

where λ is the X-ray photon wavelength. The corresponding values for the source points D1 and D4 bending magnets at 21 keV are calculated to be 7.1 µm and 7.6 µm respectively. According to Table 1 the expected nominal beam sizes in these locations are larger than the minimum resolvable beam size and similar sizes are measurable at Diamond [2].

X-ray Beam Extraction

The X-ray beam is extracted from a bending magnet and goes through a modified crotch absorber that shadows the downstream components from synchrotron radiation. The crotch absorber transmits only the defined X-ray footprint required to illuminate the pinhole aperture.

The X-ray beam is incident on a 1 mm thick aluminium window, which acts as a filter by shifting the transmitted spectrum towards higher energies and reducing the total beam power from approximately 16.7 W to 1.4 W for the D1 magnet and from 12.4 W to 0.66 W for the D4 magnet. The spectrums of the bending magnets after the 1 mm aluminium window, for a beam energy of 3.5 GeV, are shown and compared with those of Diamond at a beam energy of 3 GeV in Fig. 2. Calculations were performed by XOP [6] by adjusting the horizontal acceptance to 0.37 mrad and 0.33 mrad for D1 and D4 accordingly in order to achieve a 1 mm wide horizontal footprint in the pinhole aperture plane. The cooling strategy for the aluminium window has not yet been finalized; however, the potential options under consideration are: (i) no heatsink, (ii) an integrated heatsink machined into the flange with natural convection, (iii) an integrated heatsink machined into the flange with forced convection, (iv) an external heatsink, and (v) active water cooling.

One potential improvement to the system to minimise the attenuation of the transmitted power is to install a black pipe flushed with nitrogen between the pinhole assembly and the scintillation screen. According XOP calculations,
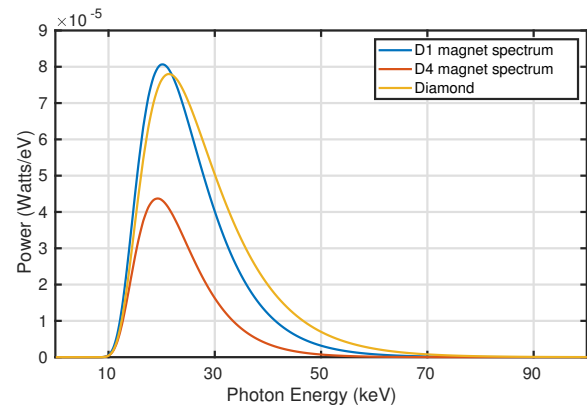

Figure 2: Transmitted spectral power distribution through a 1 mm aluminium window from D1, D4 and Diamond bending magnet using XOP.

air can attenuate the X-ray intensity by approximately 50% of its initial power after the 1 mm aluminium window from vaccumm to air, while under nitrogen the X-ray intensity stays constant.

Pinhole Apertures

A set of sixteen pinhole apertures is placed after the aluminium window. In the current design, the apertures are formed using two orthogonal stacks of 1 mm thick, 5 mm wide tungsten blades, separated by chemically etched shims with thickness of 25 µm, 50 µm, and 400 µm [7]. For nominal operation, 25 µm apertures are used as they are a good compromise between resolution and flux. For initial alignment purposes the large aperture of 400 µm × 400 µm is used.

Since only a single aperture should be illuminated at a time to avoid any interference with neighboring apertures and given that every aperture is separated from each other by a 1 mm blade, the crotch absorber has been designed with a suitable acceptance such that the radiation footprint at the plane of the pinhole apertures is not larger than 2 mm × 2 mm. In parallel, an alternative pinhole aperture assembly design is being investigated, employing C-D shaped blades to eliminate the need for shims and provide more stable and accurate aperture dimensions [8]. However, manufacturing a tungsten assembly with high tolerances has proven challenging. Electro-discharge machining (EDM) has been attempted with limited success but the process is going to repeated using a different supplier [9].

X-rays passing through air in the vicinity of tungsten cause oxidation, resulting in the accumulation of oxides that eventually block the pinhole apertures. For this reason, the pinhole assembly is held under nitrogen.

To enable the X-ray Diffractometry technique when the beam size is below the resolution of the pinhole cameras, a LIGA screen with high aspect ratio pinhole apertures will be used [10]. As this technique requires monochromatic beam, the LIGA screen will be installed in a third pinhole camera,

identical to pinhole camera 2 that will be equipped with a monochromator [4].

Motion Stages

The pinhole aperture assembly is mounted on four stages with micro stepping capability; a horizontal stage to position and retract the assembly from the photon beam; a vertical stage for alignment in the vertical plane; a rotational stage to rotate the assembly around the vertical axis; and a goniometer stage to rotate about the horizontal axis, ensuring maximum photon flux passes through the pinhole aperture (see Fig. 3). The stages and the pinhole assembly will be installed on the main girder supporting the ring magnets and vacuum vessels. Due to tight spatial constraints on the girder, a careful selection of motion stages is required to ensure they fit without interfering with other accelerator components.

A compact goniometer and a rotary stage equipped with piezo controllers and encoders to provide high repeatability, were chosen in order to meet the requirements. However, the encoders are possibly at a high risk of failure due to radiation damage. Currently, a solution with a compact cooling option for the aluminium window that allows more space on the girder is being explored in conjunction with the engineering group. This will allow the use of stepper motors that have been proven to be robust in the radiation environment. All the stages will be mounted on a common platform that can be removed from the girder for maintenance or replacement in the event of a failure, due to the limited access.
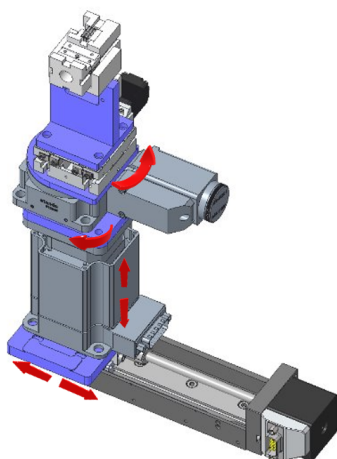

Figure 3: The set of motion stages for the alignment of the pinhole apertures with the X-ray beam.

Imaging System

The imaging system of the pinhole camera includes the scintillator, the lens and the camera sensor.

The scintillator Gadolinium aluminium gallium garnet doped with cerium (GAGG+) [11] has been studied for diagnostic applications at other facilities [12]. Previous studies at Diamond demonstrated two-fold increase in photon yield in comparison to LuAG:Ce which is used currently [9]. This will allow for better imaging of the X-ray beam at low current and enable shorter exposure times thereby reducing the contribution of jitter within images. The thickness of the scintillator is a trade off between the resulting flux and the spatial resolution of the system. Increasing the scintillator thickness enhances X-ray absorption efficiency, thus the photon flux. However, in a thick scintillator, X-rays interact and generate light at different depths within the material leading to image blurring [13]. Another requirement is that the scintillator thickness should be smaller than the depth of field of the optical system.

The current imaging system employs a Schneider-Kreuznach Componon-S 2.8/50 lens [14]. The lens requirements include a working distance of less than 10 mm, 1:1 magnification and field of view larger than 5 mm × 4 mm to allow dispersion measurements in the storage ring. Performance evaluation of alternative options including telecentric lenses (Computar 5MP, 2/3" 55 mm F2.8 Telecentric Lens [15]) and high resolution lenses as the Computar MPZ, 20MP 75 mm F3.1 model [16] were conducted in the optics lab by comparing their Modulation Transfer Function. The results indicated that none of the tested alternatives presented superior performance compared to the existing lens.

The camera attached to the lens will be the Mako G-511 GigE camera from Allied Vision with 1/1.8 Sony IMX547 CMOS sensor, resolution of 2064×2064 pixels and pixel size of 2.74 μm × 2.74 μm [17]. To enable focusing of the system remotely, the camera with the lens are going to be mounted on a linear stage with 25 mm travel range and 0.1 μm minimum incremental motion. The entire system is mounted on a pair of identical linear stages: one oriented horizontally and the other vertically, so the imaging system can be aligned to the X-ray beam.

CONCLUSION

The pinhole cameras are expected to be the workhorse for the emittance and energy spread measurement for nominal beam conditions in Diamond-II.

The main challenge for the design of the pinhole cameras for Diamond-II is the aim to increase the magnification of the system by locating the pinhole aperture closer to the source point. Higher magnification increases the projected size of the object on the sensor, enhancing spatial resolution and allowing finer features to be resolved. This has been achieved but results in a restricted area for the installation and access of the pinhole aperture assembly. Thus, the system needs to be carefully designed for compactness. Different stages that can fit within the available space, can be accessed for maintenance or replacement have the required resolution and are robust in a radiation environment have been explored.

The imaging system for Diamond-II has been designed and will consist of a GAGG scintillator that has high photon yield, the existing imaging lens a GigE camera that offers higher sensitivity and enhanced spatial resolution.

For a squeezed beam following optics correction where the beam size is below pinhole cameras resolution, X-ray diffractometry will be used as a complementary method.

REFERENCES

[1] M. Abbott *et al.*, *Diamond-II Technical Design Report*, R. P. Walker, Ed., Diamond Light Source, Didcot, UK, Jun. 2022, `https://www.diamond.ac.uk/Home/News/LatestNews/2022/14-10-22.html`

[2] C. Thomas, G. Rehm, I. Martin, and R. Bartolini, "X-Ray Pinhole Camera Resolution and Emittance Measurement", *Phys. Rev. Spec. Top. Accel Beams.*, vol. 13, no. 2, p. 022805, 2010. `doi:10.1103/PhysRevSTAB.13.022805`

[3] P. Elleaume, C. Fortgang, C. Penel, E. Tarazona, "Measuring Beam Sizes and Ultra-Small Electron Emittances Using an X-ray Pinhole Camera.", *J. Synchrotron Radiat.*, vol. 2, no. 5, pp. 209–214, 1995. `doi:10.1107/S0909049595008685`

[4] N. Vitoratou and L. Bobb, "Study of X-ray Fresnel Diffractometry for Small Beam Sizes at Diamond Light Source", in *Proc. IBIC'24*, Krakow, Poland, Sep. 2022, paper TUP58, pp. 187–190. `doi:10.18429/JACoW-IBIC2024-TUP58`

[5] L. Farvacque *et al.*, *EBS Storage Ring Technical Report*, D. Einfeld, Ed., ESRF, Grenoble, France, 2018. `https://www.esrf.fr/files/live/sites/www/files/com%20photos/About%20Us/EBS-TECHREPORT-reduced.pdf`

[6] XOP, `https://www.esrf.fr/home/UsersAndScience/support-and-infrastructure/software/data-analysis/OurSoftware/xop2.4/documentation.html`

[7] L. M. Bobb, A. F. D. Morgan, and G. Rehm, "Performance Evaluation of Molybdenum Blades in an X-ray Pinhole Camera", in *Proc. IBIC'16*, Barcelona, Spain, Sep. 2016, pp. 795–798. `doi:10.18429/JACoW-IBIC2016-WEPG63`

[8] F. Ewald, "Emittance diagnostics at ESRF-EBS using the X-ray Pinhole Camera", presented in *ELETTRA 2.0 Workshop on Optical Diagnostics for Low-Emittance Storage Rings*, Mar. 2022. `https://indico.psi.ch/event/12679/contributions/34867/`

[9] S. B. Burholt, L. Bobb, and N. Vitoratou, "Performance Evaluation of GAGG+ and Tungsten Carbide Blades in an X-ray Pinhole Camera", in *Proc. IBIC'23*, Saskatoon, Canada, Sep. 2023, pp. 382–386. `doi:10.18429/JACoW-IBIC2023-WEP020`

[10] N. Vitoratou, L. Bobb, A. Last, and G. Rehm, "X-Ray Pinhole Camera Spatial Resolution Using High Aspect Ratio LIGA Pinhole Apertures", in *Proc. IBIC'22*, Kraków, Poland, Sep. 2022, pp. 71–75. `doi:10.18429/JACoW-IBIC2022-MOP18`

[11] Specific GAGG+ and other materials, `https://www.crytur.cz/materials/gagg/`

[12] G. Kube, C. Behrens, C. Gerth, B. Schmidt, W. Lauth, and M. Yan, "Inorganic Scintillators for Particle Beam Profile Diagnostics of Highly Brilliant and Highly Energetic Electron Beams", in *Proc. IPAC'12*, New Orleans, LA, USA, May 2012, paper WEOAA02, pp. 2119–2121.

[13] T. Martin, A. Koch, "Recent developments in X-ray imaging with micrometer spatial resolution", *J. Synchrotron Radiat.*, vol. 13, pp. 180–194, 2006. `doi:10.1107/S0909049506000550`

[14] Componon-S 2.8/50, `https://ftp.stemmer-imaging.com/webdavs/docmanager/141084-Schneider-Componon-S-12-50-2.8.pdf`

[15] V7531-MPZ, `https://www.computar.com/products/v7531-mpz`

[16] TEC-55, `https://www.computar.com/products/tec-55`

[17] Mako G-511, `https://www.alliedvision.com/en/camera-selector/detail/mako/g-511/`